Evaluation of Historical and Future Cool Season Precipitation over the Eastern United States and Western Atlantic Storm Track Using CMIP5 Models

KELLY LOMBARDO

University of Connecticut, Groton, Connecticut

BRIAN A. COLLE AND ZHENHAI ZHANG

School of Marine and Atmospheric Sciences, Stony Brook University, Stony Brook, New York

(Manuscript received 13 May 2014, in final form 8 October 2014)

ABSTRACT

This study analyzed the contribution of cyclones to projected changes in cool season (1 November–31 March) precipitation over the eastern United States and western North Atlantic Ocean. First, global climate model simulations from phase 5 of the Coupled Model Intercomparison Project (CMIP5) were compared to Global Precipitation Climatology Project (GPCP) and Climate Prediction Center (CPC) precipitation analyses for the period 1979–2004. The CMIP5 ensemble mean realistically reproduced the historical distribution of regional precipitation with no discernable effect because of model spatial resolution. Subsequently, the projected changes in precipitation on cyclone and noncyclone days under the representative concentration pathway 8.5 (RCP8.5) scenario were quantified. While precipitation on both types of days was projected to increase, the increase on noncyclone days (23%) was greater than the increase on cyclone days (12%). The increase in precipitation on cyclone days occurred despite a decrease in the number of cyclone days. This increase can be attributed primarily to a shift toward more frequent extreme precipitation events coupled with a decline in light precipitation events.

1. Introduction

Heavy precipitation from extratropical cyclones can have tremendous societal impacts along the eastern United States, ranging from heavy snow (Novak et al. 2008) to inland and coastal flooding (Colle et al. 2008). For example, the 8–10 February 2013 blizzard brought more than 30 in. (~76 cm) of snow to coastal New York and Connecticut, which led to a loss of power for thousands of northeastern U.S. residents and major disruptions to national airlines (http://www.erh.noaa.gov/okx/StormEvents/storm02082013.html). The 7–8 November and 26–27 December 2012 nor'easters created similar damage across the region, with wind gusts as high as 27 m s^{-1} (http://www.erh.noaa.gov/okx/StormEvents/storm12262012.html) in conjunction with snowfall and coastal flooding.

Future regional changes in precipitation intensity and frequency associated with extratropical cyclones depend on the spatial and temporal variations in atmospheric moisture as well as the change in the position and intensity of the North Atlantic storm track. Globally, mean precipitation rates associated with midlatitude cyclones have been shown to rise with increasing atmospheric moisture and cyclone strength (Field and Wood 2007). The regional variations in precipitation associated with cyclones are less clear, especially near land–water transition zones, such as the eastern United States and western Atlantic Ocean.

As the global tropospheric air temperature warms in a future climate, the Clausius–Clapeyron (CC) equation indicates that the saturation vapor pressure will increase at a rate of 7% K^{-1} (Held and Soden 2006). Such increases in the lower-tropospheric water vapor will impact the hydrological cycle, including the quantity and intensity of precipitation globally (Trenberth et al. 2003). Using an ensemble of eight climate models, Wetherald and Manabe (2002) illustrated that the global precipitation rate is projected to increase by 5.2% by the middle

Corresponding author address: Kelly Lombardo, Department of Marine Sciences, University of Connecticut, 1080 Shennecossett Road, Groton, CT 06340.
E-mail: kelly.lombardo@uconn.edu

DOI: 10.1175/JCLI-D-14-00343.1

of the twenty-first century (2035–65); however, there are regional variations within these global precipitation changes. The annual precipitation rate in high latitudes is projected to increase more rapidly than the rate of evaporation, while the opposite is projected for the subtropics (Manabe and Stouffer 1980; Manabe and Wetherald 1980; Meehl et al. 2007; Wentz et al. 2007). The transition zone between the positive precipitation minus evaporation ($P - E$) in the high latitudes and negative $P - E$ in the subtropics lies within the midlatitudes, suggesting large regional precipitation variability within this hemispheric latitudinal band (Kutzbach et al. 2005).

While understanding latitudinal variations in precipitation changes is important, extreme precipitation events on synoptic time scales can have more dramatic impacts locally. Pfahl and Wernli (2012) illustrated that in the historical European Centre for Medium-Range Weather Forecasts (ECMWF) Interim Re-Analysis (ERA-Interim) data, as much as 80% of extreme precipitation events, defined as the 99th percentile of 6-hourly precipitation, is directly related to cyclones over some regions (e.g., Newfoundland, Japan, South China Sea, and Mediterranean Sea). Furthermore, the number of extreme precipitation events (upper 0.1%–10%) across the globe is anticipated to rise as much as 6%–40% at the expense of lighter events, in part because of the projected increase in lower-tropospheric moisture (Allen and Ingram 2002; Semenov and Bengtsson 2002; O'Gorman and Schneider 2009), and GCMs may be underestimating this increase (Allan and Soden 2008). While cyclones have been shown to be associated with extreme precipitation events, the contribution of cyclones, if any, to future precipitation increases in extreme events is unknown.

Given large regional variability in the distribution of precipitation, it is imperative that historical and future precipitation trends are evaluated over smaller subregions within the midlatitudes, such as the eastern United States. There has been an increasing trend in both total accumulated annual northeastern U.S. precipitation as well as the frequency of the heaviest precipitation events over the region during the last century (Wake and Markham 2005; Griffiths and Bradley 2007; Brown et al. 2010; Insaf et al. 2013; Kunkel et al. 2013a,b). On average, annual accumulated U.S. Northeast precipitation has increased 8% (~85 mm) over the past 100 yr, with a 2% increase in the number of events producing greater than ~50 mm over a 48-h period (Wake and Markham 2005). Kunkel et al. (2013a) found that annual conditions over the Northeast have been becoming significantly wetter from 1957 to 2010. This increasing trend was observed in both observations and GCM ensembles during the December–February (DJF) winter months (Hayhoe et al. 2007).

Several studies have shown the ability of the global climate models to realistically represent trends in regional historical precipitation (Horton et al. 2011; DeAngelis et al. 2013; Kunkel et al. 2013b), which provides confidence in their use when evaluating future precipitation trends. Using output from phase 3 of the Coupled Model Intercomparison Project (CMIP3; Annan and Hargreaves 2011), DeAngelis et al. (2013) illustrated how the CMIP3 ensemble realistically represented the seasonal cycle of heavy precipitation over the Northeast. Using a 15-member CMIP3 ensemble, Kunkel et al. (2013b) found a statistically significant increase (3%–9%) in Northeast annual accumulated precipitation under the Special Report on Emissions Scenarios A2 greenhouse gas (GHG) emissions scenario between 1971 and 1999, while a similar increase was projected under the A1B scenario as well (Horton et al. 2011).

The global climate models project an increase in the magnitude and frequency of future precipitation over the northeastern United States (Semenov and Bengtsson 2002; Hayhoe et al. 2007; Kharin et al. 2007; Horton et al. 2011; Kunkel et al. 2013a; Scoccimarro et al. 2013; Maloney et al. 2014). Using the single ECHAM4/Ocean Isopycnal Model version 3 (OPYC3) global climate model (GCM), Semenov and Bengtsson (2002) showed a rising trend in eastern U.S. accumulated precipitation of 10%–20% $(100\,\text{yr})^{-1}$ through the twenty-first century. Kunkel et al. (2013a) showed using an 11-member regional ensemble from the North American Regional Climate Change Assessment Program (NARCCAP; Mearns et al. 2009) that the largest increase in accumulated Northeast precipitation occurs during DJF (20%). Hayhoe et al. (2007) illustrated a slightly larger (30%) increase in DJF Northeast precipitation, using an ensemble of GCMs from the International Panel on Climate Change (IPCC) Fourth Assessment Report (AR4). Using the next generation of Coupled Model Intercomparison Project (CMIP) models [phase 5 of CMIP (CMIP5); Taylor et al. 2012], the magnitude of the heaviest east coast DJF precipitation events are projected to increase by 30%–40% by the 2061–2100 period, with the magnitude of the most intense precipitation events projected to rise faster than the overall mean (Scoccimarro et al. 2013). Maloney et al. (2014) illustrated that the increase in the frequency of northeastern U.S. precipitation is projected to be as much as 400% for the heaviest precipitation events ($>25\,\text{mm day}^{-1}$), although the sample size was small (5–25 events over 30 yr).

Future variations in regional precipitation are in part a function of the midlatitude cyclone track, frequency, and intensity. During the boreal winter, the Northern Hemisphere extratropical storm track is projected to shift poleward of its current location (Bengtsson et al. 2006),

with a statistically significant increase in cumulative precipitation within the cyclone track (Bengtsson et al. 2009). Across the North Atlantic basin, this increase in precipitation is projected to occur regardless of the reduction in the number of cyclones across the basin (Bengtsson et al. 2006; Chang 2013; Zappa et al. 2013). While the basinwide trend suggests fewer cyclones, it is important to consider smaller regional variations, especially near highly populated coastal areas. Variations in coastal cyclone behavior will have dramatic societal impacts and may not follow the larger trend. For example, using an ensemble of CMIP5 members, Colle et al. (2013) found a 10%–30% decrease in future cool season cyclone activity over the western North Atlantic but a 10%–20% increase in cyclone activity over the eastern United States. It is unclear how these opposing changes in cyclone activity will impact both future mean and extreme precipitation over these geographically varying subdomains of the eastern United States.

This study evaluates future projections in cool season precipitation over two adjacent and topographically varying regions, namely the eastern U.S. coastal plain and the western Atlantic coastal ocean. Precipitation projections associated with cyclones are highlighted and compared to future projections in the cyclone frequency over the regions of interest. Future projections in the frequency of light, moderate, and extreme precipitation events associated with coastal cyclones are presented as well. The methodology and data used in this study is described in section 2. Section 3 discusses the results of the precipitation analyses while section 4 provides discussion and summary of future projections in eastern U.S. and western Atlantic precipitation.

2. Data and methods

The CMIP5 multimodel ensemble provides a standardized set of atmosphere–ocean global model simulations to evaluate future variations in global and regional climate. In the current study, daily precipitation was obtained and analyzed for 14 CMIP5 members (Table 1). The CMIP5 ensemble members were selected because of the availability of daily precipitation output over the period of interest for this study. CMIP5 model output are available for a historical time period, spanning the mid-nineteenth century through 2005, as well as a future time period, which extends to 2100. The long-term historical simulations are initialized from a preindustrial control and forced by observed time-evolving atmospheric compositions (reflecting both anthropogenic and natural sources) and land cover. Long-term future projection simulations are forced by prescribed levels of total radiative forcing, defined as representative concentration pathways (RCPs), determined by a cumulative measure of human emissions of greenhouse gases, air pollution, and land use. This study used the high representative concentration pathway, which allows the radiative forcing to increase to 8.5 W m^{-2} by the year 2100 (RCP8.5). CMIP5 precipitation fields were evaluated over the cool season, defined as 1 November–31 March, for each individual year as well as for four longer time periods, defined as the historical period (1979/80–2004/05), the early twenty-first century (2009/10–38/39), the mid-twenty-first century (2039/40–68/69), and the late twenty-first century (2069/70–98/99).

Historical CMIP5 precipitation was compared to observational precipitation products to gain confidence in using the GCMs to analyze future projections. At present, there is no definitive precipitation product spanning both land and large bodies of water that has gained acceptance as the most accurate, with the largest discrepancies between datasets occurring over oceanic regions. Subsequently, a common approach to evaluating these data is through comparisons of multiple sources to determine their strengths and weaknesses (i.e., Yin et al. 2004; Arkin et al. 2010). While certain products have been identified as more reliable in specific regions of the globe, such as the high latitudes or the tropics, none have been defined as the most reliable over midlatitudes, including the eastern United States and western Atlantic. As such, the present study used three precipitation products to evaluate the performance of the CMIP5 output during the historical period: Global Precipitation Climate Project (GPCP; Adler et al. 2003) monthly averaged precipitation data available at 2.5° × 2.5° resolution provided by the National Oceanic and Atmospheric Administration (NOAA)/Office of Oceanic and Atmospheric Research (OAR)/Earth System Research Laboratory (ESRL)/Physical Sciences Division (PSD), Boulder, Colorado, obtained from their website (http://www.esrl.noaa.gov/psd); Climate Prediction Center (CPC) Merged Analysis of Precipitation (CMAP; Xie and Arkin 1996, 1997) monthly averaged precipitation data available at 2.5° × 2.5° resolution provided by the National Center for Atmospheric Research (NCAR), retrieved from their website (https://climatedataguide.ucar.edu/climate-data/cpc-merged-analysis-precipitation-cmap); and CPC unified daily averaged precipitation data (Higgins et al. 1996, 2000) available over the continental United States at 0.25° × 0.25° resolution, provided by the NOAA/OAR/ESRL/PSD and obtained from their website (http://www.esrl.noaa.gov/psd). The GPCP product combines satellite estimates of precipitation and rain gauge data; the CMAP product is derived from satellite, rain gauge, and reanalysis precipitation; and the CPC unified product is primarily based on rain gauge data.

All CMIP5 model output and analyses products were interpolated to a common 1° × 1° latitude–longitude

TABLE 1. CMIP5 models included in the precipitation analysis.

Model acronym	Model expanded name	Modeling center	Horizontal resolution (lon × lat)	No. of vertical levels	Reference
BCC-CSM1.1	Beijing Climate Center (BCC), Climate System Model, version 1.1	BCC, China Meteorological Administration	2.8° × 2.8°	26	Xin et al. (2012)
CanESM2	Second Generation Canadian Earth System Model	Canadian Centre for Climate Modelling and Analysis	2.8° × 2.8°	35	Arora et al. (2011)
CCSM4	Community Climate System Model, version 4	National Center for Atmospheric Research	1.25° × 0.94°	26	Gent et al. (2011)
CNRM-CM5.1	Centre National de Recherches Météorologiques (CNRM) Coupled Global Climate Model, version 5.1	CNRM/Centre Européen de Recherche et Formation Avancée en Calcul Scientifique	1.4° × 1.4°	31	Voldoire et al. (2013)
CSIRO Mk3.6	Commonwealth Scientific and Industrial Research Organisation (CSIRO) Mark 3.6	CSIRO in collaboration with Queensland Climate Change Centre of Excellence	1.8° × 1.8°	18	Rotstayn et al. (2010)
GFDL CM3	Geophysical Fluid Dynamics Laboratory (GFDL) Climate Model, version 3	NOAA/GFDL	2.5° × 2.0°	48	Donner et al. (2011)
GFDL-ESM2M	GFDL Earth System Model with Modular Ocean Model, version 4 (MOM4) component	NOAA/GFDL	2.5° × 2.0°	48	Donner et al. (2011)
HadGEM2-ES	Hadley Centre Global Environment Model, version 2—Earth System	Met Office Hadley Centre	1.875° × 1.25°	60	Jones et al. (2011)
INM-CM4	Institute of Numerical Mathematics (INM) Coupled Model, version 4	Institute of Numerical Mathematics	2.0° × 1.5°	21	Volodin et al. (2010)
IPSL-CM5A-LR	L'Institut Pierre-Simon Laplace (IPSL) Coupled Model, version 5A, low resolution	L'Institut Pierre-Simon Laplace	3.75° × 1.8°	39	Dufresne et al. (2013)
MIROC5	Model for Interdisciplinary Research on Climate (MIROC), version 5	Atmosphere and Ocean Research Institute (University of Tokyo), National Institute for Environmental Studies (NIES), and Japan Agency for Marine-Earth Science and Technology (JAMSTEC)	1.4° × 1.4°	40	Watanabe et al. (2010)
MIROC-ESM	MIROC, Earth System Model	JAMSTEC, Atmosphere and Ocean Research Institute (University of Tokyo), and NIES	2.8° × 2.8°	80	Watanabe et al. (2010)
MRI-CGCM3	Meteorological Research Institute (MRI) Coupled Atmosphere–Ocean General Circulation Model, version 3	Meteorological Research Institute	1.1° × 1.1°	48	Yukimoto et al. (2012)
NorESM1-M	Norwegian Earth System Model, version 1 (intermediate resolution)	Norwegian Climate Center	2.5° × 1.9°	26	Zhang et al. (2012)

grid before performing the analyses, as in Chen and Knutson (2008). A bilinear interpolation scheme was used for the interpolation, since the interpolation was from a coarser grid to a finer grid.

Historical and future precipitation analyses were performed over a large eastern U.S.–western Atlantic domain, as well as two smaller regions, a U.S. East Coast land (ECL) and East Coast water (ECW) domain (Fig. 1),

as in Colle et al. (2013). This provided an opportunity to evaluate the relationship between cyclone frequency and precipitation. Precipitation was analyzed for the complete cool season (November–March) as well as for cool season "cyclone days" only. A cyclone day was defined as a day during which the center of the cyclone was located within the domain of interest (i.e., ECL and ECW). Cyclones were identified using the 6-hourly global mean sea level pressure from the CMIP5 ensemble. Given the 6-hourly analyses used, a cyclone day was defined as 0000–1800 UTC. Mean sea level pressure (MSLP) was used to track surface cyclones over the eastern U.S. and western Atlantic storm track using the tracking scheme developed by Hodges (1994, 1995), following the methods of Colle et al. (2013). Using this method, the cyclones were identified as local minima in the mean sea level pressure fields with at least one closed MSLP contour, a minimum lifetime of 24 h, and a minimum spatial movement of 1000 km over the lifetime. Furthermore, "cyclone counts" were obtained using this method, by counting the number of cyclones observed within the ECL and ECW domains.

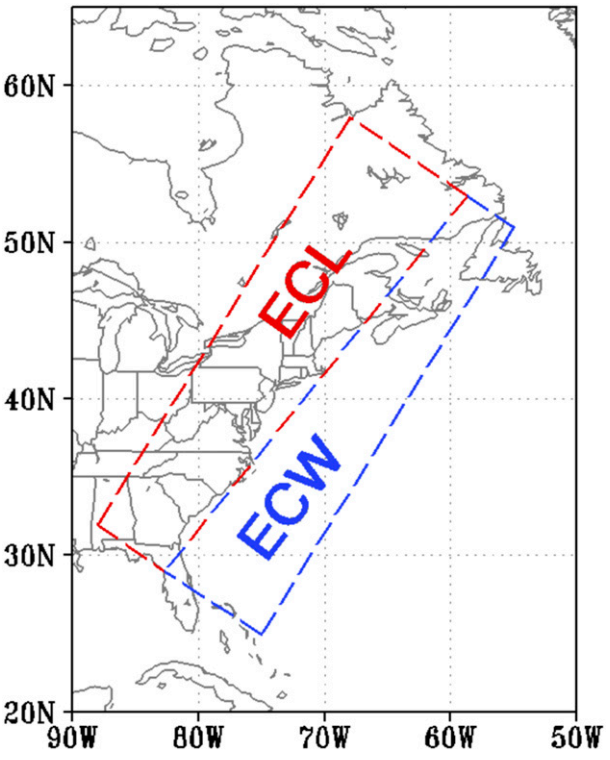

FIG. 1. Map illustrating the ECL (red) and ECW (blue) domains used in the current study.

3. Results

a. Historical precipitation

Figure 2a illustrates the CMIP5 mean precipitation and standard deviation for 14 CMIP5 members over the historical (1979–2004) cool season (November–March). The maximum in precipitation is within the northwestern Atlantic storm track, with a maximum value ranging from 975 to 1050 mm of precipitation per season and a standard deviation of 100–200 mm season^{-1}. Over the eastern United States, precipitation values range from 450 to 525 mm season^{-1} in the southeastern part of the United States, decreasing to 375–450 mm season^{-1} in the northeastern United States, with higher values along the coastal region (450–525 mm season^{-1}).

The CMIP5 historical mean precipitation is compared to three precipitation products to assess its ability to accurately represent the distribution and magnitude of past precipitation. Figures 2b–d illustrate the mean distribution of three different precipitation products over the historical cool season, while Fig. 3 quantitatively shows the spatial difference in the means of the CMIP5 and the precipitation products (CMIP5 minus product). The GPCP precipitation product has a maximum in precipitation over the northwestern Atlantic storm track (975–1050 mm season^{-1}; Fig. 2b) similar to the CMIP5 mean, though values within the storm track are smaller by ~80–160 mm season^{-1} in the CMIP5 mean (Fig. 3a). In the southeastern United States, seasonal GPCP precipitation values are 240–320 mm larger than the CMIP5 mean (Fig. 3a). Over the northeastern United States, the spatial distribution of precipitation in the GPCP is similar to the CMIP5 mean, with values 80–160 mm larger than the CMIP5 mean (Fig. 2a). To quantify the spatial correlation between the two fields, the correlation coefficient between the GPCP and CMIP5 mean was calculated using each grid point over the combined ECL–ECW domain. The correlation coefficient returned a value of 0.95, indicating that the spatial distribution of the GPCP and CMIP5 mean are well correlated over the region of interest.

For the CMAP derived precipitation, the precipitation maximum over the northwestern Atlantic has a smaller spatial area than the CMIP5 mean, though the maximum values are similar (Figs. 2a,c). As a result, the CMIP5 mean shows more precipitation per season within the northwestern Atlantic storm track, especially off Cape Hatteras (240–320 mm; Fig. 3b). In the southeastern United States, CMAP values are 80–160 mm larger than the CMIP5 average, though CMAP values in the northeastern United States are as much as 80–160 mm less (Fig. 3b). Quantifying the correlation between the CMAP product and the CMIP5 mean over the ECL–ECW combined domain, the correlation coefficient is 0.93, indicating that the spatial distribution of the two precipitation fields are well correlated.

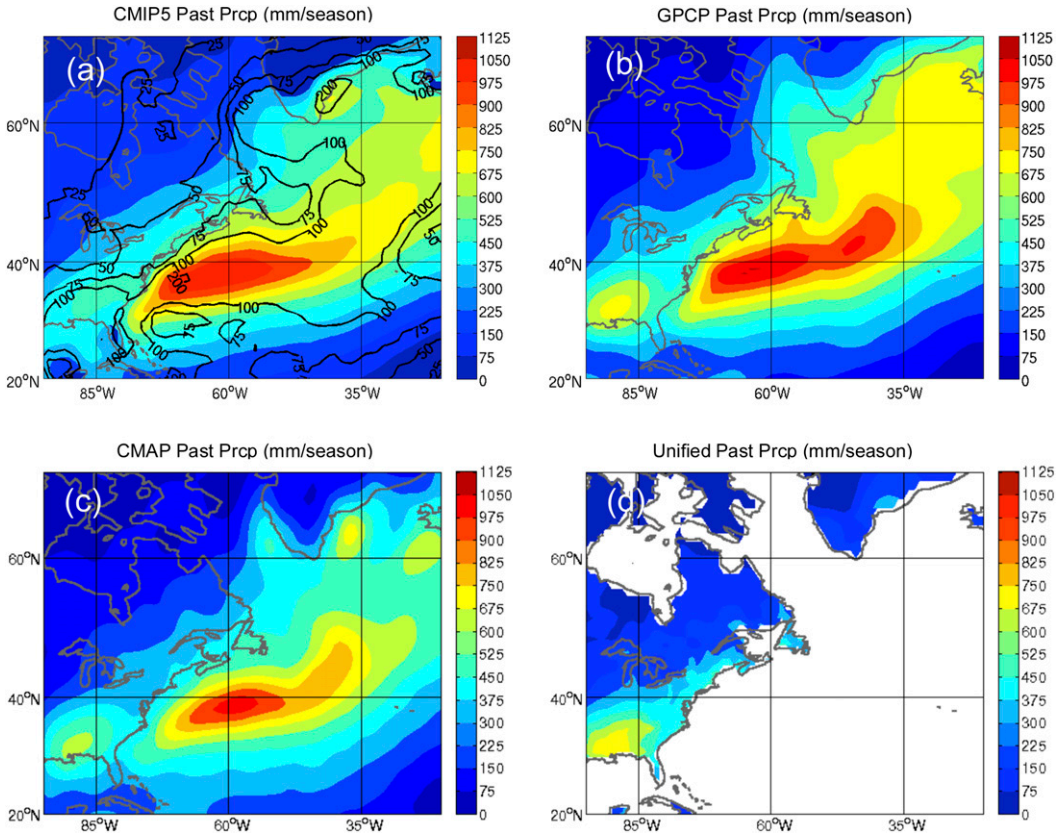

FIG. 2. Mean cool season (November–March) precipitation (shaded; mm season^{-1}) for the historical period (1979–2004) for (a) 14 CMIP5 members from Table 1, (b) the GPCP precipitation product, (c) the CMAP precipitation product, and (d) CPC unified precipitation product. Solid black lines in (a) represent the standard deviation of the CMIP5 mean, contoured every 25 mm season^{-1} from 25 to 100 mm season^{-1} and every 100 mm season^{-1} above 100 mm season^{-1}.

The fine resolution of the CPC unified precipitation product makes it a valuable resource over land, despite the lack of data over the ocean. In the southeastern United States, the CPC unified product has a cool season precipitation maximum of 675–750 mm (Fig. 2d), 240–320 mm larger than the CMIP5 mean (Fig. 3c). Over the northeastern states, there is little difference between the CPC unified product (300–450 mm season^{-1}) and CMIP5 data, though the CMIP5 data slightly overestimates precipitation in localized regions in New Brunswick and Newfoundland. Over the southeastern United States, the CPC unified data shows as much as 320–400 mm season^{-1} of precipitation more than the CMIP5 mean (Fig. 3c).

Comparisons of the CMIP5 precipitation to the observations (Fig. 3d) illustrates that mean values over the northern part of the western Atlantic storm track fall between the two observationally based products available over water, with more precipitation than the CMAP and less than the GPCP. The CMIP5 data overestimates precipitation over the offshore storm-track entrance between approximately 25° and 35°N. Over the land, the CMIP5 data consistently underrepresents southeastern U.S. precipitation but has values between the two observational products over the Northeast and portions of the mid-Atlantic.

The performance of the individual CMIP5 members used in the historical analysis was evaluated with respect to the CMAP and GPCP analyses products over the combined ECL–ECW domain, defined as the EC domain (Table 2). The root-mean-square error (RMSE) was calculated between the individual model members used in this study and both the analyses products. This provides a measure of the average error between the models and the observational analyses within the domain. The normalized RMSE was calculated as well, normalized by the average of the model and analysis product, describing the percent error between the model and analyses. Performance of the CMIP5 members was evaluated based on the resolution of the model grids, as defined by Colle et al. (2013). The mean, RMSE, and normalized RMSE were calculated

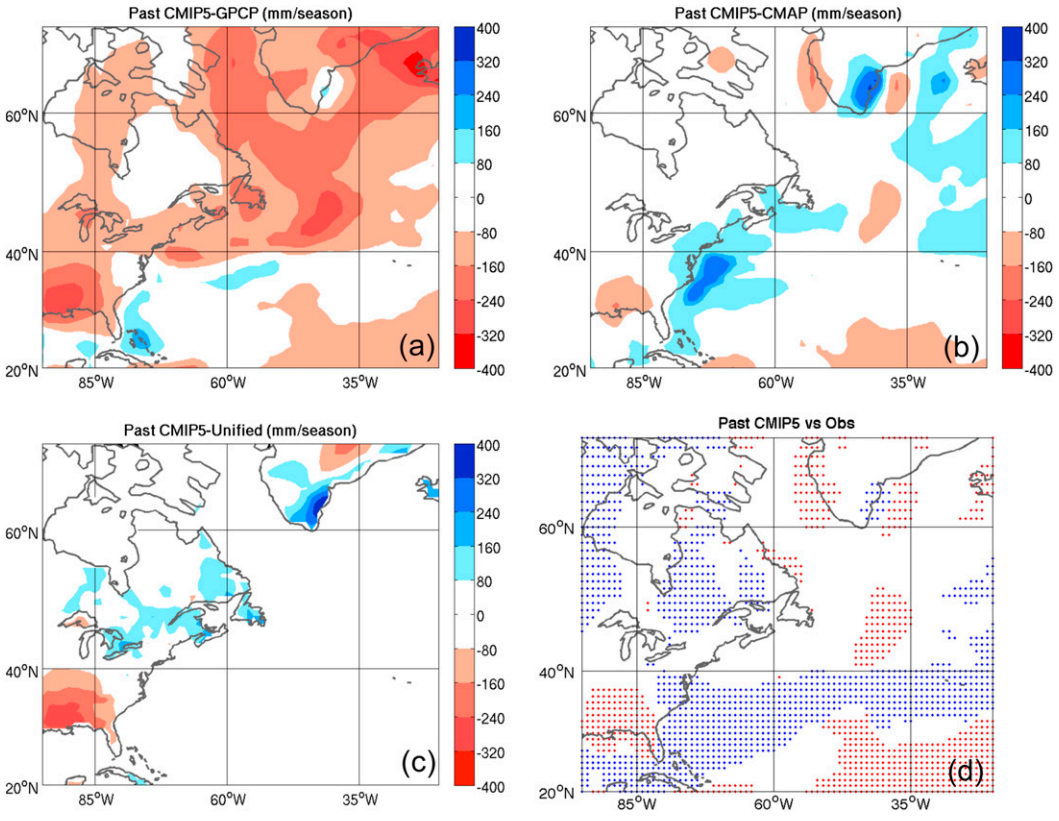

FIG. 3. Difference plots of the historical cool season CMIP5 mean precipitation minus the cool season historical mean precipitation of the (a) GPCP, (b) CMAP, and (c) CPC unified data. Differences are shaded every 80 mm season^{-1}. (d) CMIP5 mean compared to both GPCP and CMAP data. Blue (red) dots represent locations where the CMIP5 mean is larger (smaller) than both the GPCP and CMAP data.

between the precipitation analyses products as well, to highlight the difference between the two analyses products.

The mean precipitation over the EC domain for the CMIP5 ensemble members ranges from 451.5 to 639.7 mm season^{-1} m^{-2}, with a CMIP5 mean precipitation value of 549.5 mm season^{-1} m^{-2} (Table 2). The CMIP5 mean falls between the mean CMAP (454.8 mm season^{-1} m^{-2}) and GPCP (557.1 mm season^{-1} m^{-2}) average values. The RMSE between the CMIP5 mean and the CMAP is larger (122.7 mm season^{-1} m^{-2}) than the GPCP analyses (69.8 mm season^{-1} m^{-2}), though there is variability in the performance of the individual members. For example, the RMSE between the CMAP and the CSIRO Mk3.6, MIROC-ESM, and NorESM1-M is smaller than the RMSE between these three members and the GPCP data. Complementarily, the normalized RMSE between the CMIP5 mean and the CMAP is larger (24.4%) than the GPCP analyses (12.6%), though the normalized RMSE between the CSIRO Mk3.6, MIROC-ESM, and NorESM1-M members and the CMAP is smaller than for the GPCP.

Model performance was evaluated based on grid resolution, with the relatively high-resolution models in italics and the relatively low-resolution models in bold, with the CMIP5 mean included as well in Table 2. Several of the CMIP5 members with relatively low resolutions have smaller RMSE and normalized RMSE than members with finer-resolution grids. For example, comparing the GCMs to the GPCP, the lower-resolution GFDL-ESM2M, BCC-CSM1.1, and IPSL-CM5A-LR perform better than the higher-resolution CNRM-CM5.1, MRI-CGCM3, MIROC5, and HadGEM2-ES. Comparing the GCMs to the CMAP yields similar results, with the NorESM1-M, BCC-CSM1.1, GFDL-ESM2M, and IPSL-CM5A-LR performing better than the CNRM-CM5.1, MRI-CGCM3, MIROC5, and HadGEM2-ES.

Figure 4 illustrates cool season historical (1979–2005) precipitation days binned according to daily precipitation accumulation thresholds for the ECL and ECW domains. The ECL and ECW domains were evaluated separately to highlight the differences between the adjacent land and water domains, to emphasize the variability across this relatively small region. Over ECL, there are approximately 790 days with a precipitation accumulation of <0.5 mm day^{-1} m^{-2} for the ensemble mean (Fig. 4a).

TABLE 2. Mean precipitation averaged over the East Coast domain (column 2); RMSE of each CMIP5 member based on the CMAP (column 3) and GPCP (column 4) analyses products (mm season^{-1} m^{-2}); and RMSE normalized by the average of the model member and CMAP (column 5) and GPCP (column 6) analyses products. Higher-resolution models and data are italicized and lower-resolution models and data are in boldface, as defined by Colle et al. (2013). The CMAP and GPCP mean, the RMSE between the analyses products, and the RMSE normalized by the average of the analyses products are shown in the bottom row.

Model	Model mean	CMAP RMSE	GPCP RMSE	CMAP normalized RMSE (%)	GPCP normalized RMSE (%)
BCC-CSM1.1	**502.3**	**96.3**	**87.2**	**20.1**	**16.5**
CanESM2	542.0	113.4	89.1	22.8	16.2
CCSM4	*524.2*	*136.5*	*100.3*	*27.9*	*18.6*
CNRM-CM5.1	*563.4*	*165.8*	*109.2*	*32.7*	*19.5*
CSIRO Mk3.6	515.2	104.5	116.9	21.6	21.8
GFDL CM3	572.5	150.4	67.1	29.3	11.9
GFDL-ESM2M	**539.2**	**116.8**	**78.0**	**23.5**	**14.2**
HadGEM2-ES	*639.7*	*259.0*	*165.9*	*47.3*	*27.7*
INM-CM4	**600.2**	**169.2**	**119.8**	**32.1**	**20.7**
IPSL-CM5A-LR	**548.1**	**147.2**	**107.8**	**29.4**	**19.5**
MIROC5	*606.0*	*215.2*	*133.1*	*40.6*	*22.9*
MIROC-ESM	489.2	93.2	131.1	19.8	25.1
MRI-CGCM3	*599.1*	*194.6*	*132.4*	*36.9*	*22.9*
NorESM1-M	**451.5**	**79.1**	**147.2**	**17.5**	**29.2**
CMIP5 mean	549.5	122.7	69.8	24.4	12.6
CMIP5 low-resolution avg	528.3	121.7	108.0	24.5	20.0
CMIP5 high-resolution avg	586.5	194.2	128.8	37.1	22.3
	CMAP mean	GPCP mean	RMSE	Normalized RMSE (%)	
Analyses	454.8	557.1	134.5	26.6	

The spread in the number of these relatively weak precipitation events range from about 580 (INM-CM4) to about 1160 (NorESM1-M), with the CSIRO Mk3.6 model as the low outlier (151 events). For 0.5–1.5 mm day^{-1} events, the mean increases to 1135 days, with a smaller spread among the members. For more moderate and heavy precipitation events, the number systematically decreases from 478 (3.5–5.5 mm day^{-1}) to 159 (7.5–9.5 mm day^{-1}) events. For the top 5% of precipitation events (>9.5 mm day^{-1}), there are 180 events in the CMIP5 mean, with a spread ranging from 78 (NorESM1-M) to 277 (INM-CM4) days.

Over the ECW domain, the distribution of the magnitude of precipitation events is similar to the land domain, though there are noticeably fewer (409 events; 48% less) of the lightest precipitation events (<0.5 mm day^{-1}) and

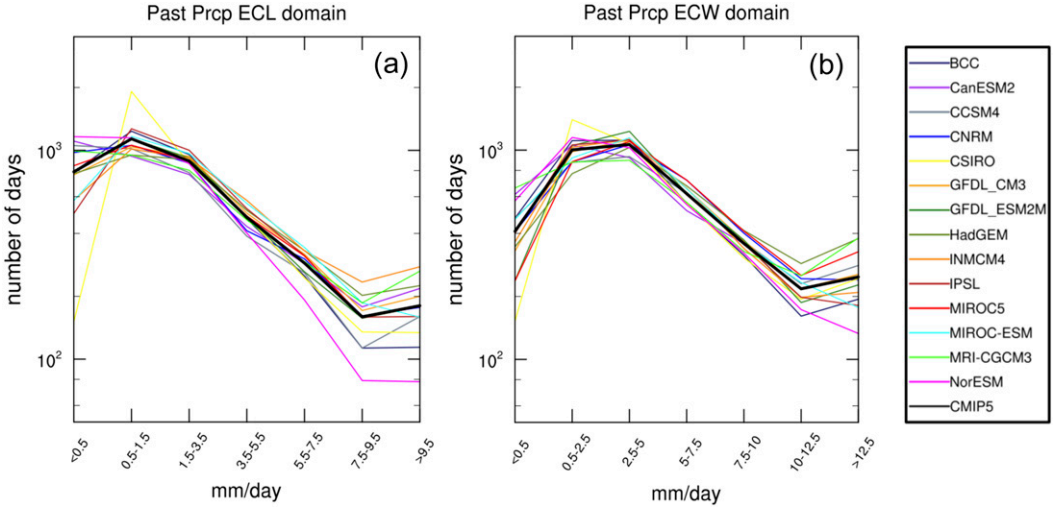

FIG. 4. Daily historical (1979–2005) precipitation distribution for 14 CMIP5 members from Table 1 (solid colored lines) and the CMIP5 mean (thick solid black line) for the (a) ECL and (b) ECW domains. The 95th percentile values are represented by daily accumulations of >9.5 mm day^{-1} in (a) and >12.5 mm day^{-1} in (b).

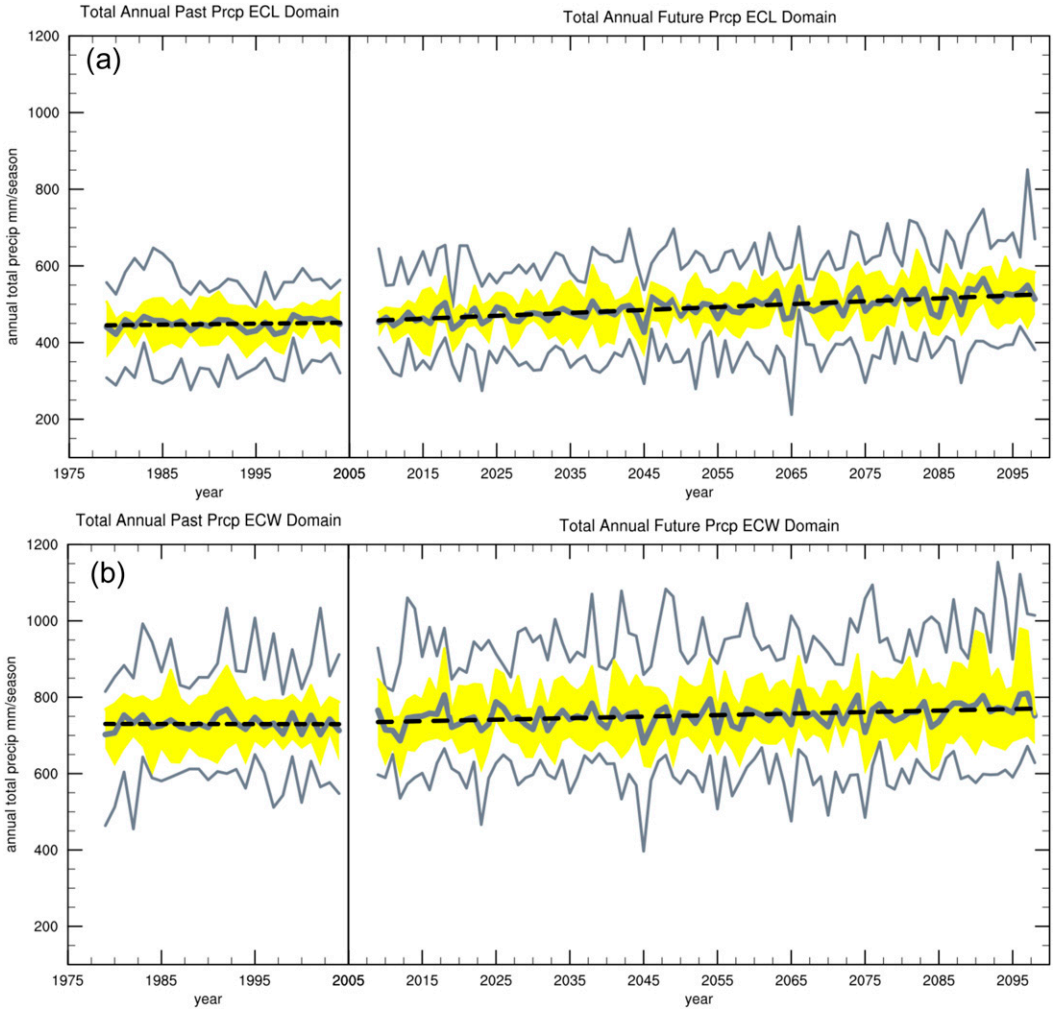

FIG. 5. Total annual precipitation (mm season^{-1}) for all cool season (November–March) days for the (a) ECL and (b) ECW domains, for 11 of the 14 CMIP5 models listed in Table 1. The thick gray line is the CMIP5 mean; the top and bottom thin gray lines are the max and min annual totals, respectively; and the yellow shading marks the interquartile range. The black dashed line is the trend in the CMIP5 mean. Models include BCC-CSM1.1, CCSM4, CNRM-CM5.1, GFDL-ESM2M, HadGEM2-ES, INM-CM4, IPSL-CM5A-LR, MIROC5, MIROC-ESM, MRI-CGCM3, and NorESM1-M.

a larger number (56 events; 25% more) of the top 5% of precipitation events (>12.5 mm day^{-1}; Fig. 4b). The spread among CMIP5 members for the lightest events over the ocean domain (from 152 for CSIRO Mk3.6 to 659 for MRI-CGCM3) is similar to that over the land domain, with a larger spread over the ECW for the top 5% of events (>12.5 mm day^{-1}; from 133 for NorESM1-M to 378 for HadGEM2-ES).

b. *Trends in regional precipitation*

1) TOTAL REGIONAL COOL SEASON PRECIPITATION

Total annual precipitation during the historical (1979–2004) and future (2009–98) periods for the ECL and ECW domains is illustrated in Fig. 5. From Table 1, 11 of the 14 CMIP5 models were used for this analysis to allow for comparisons with the cyclone analyses from Colle et al. (2013). Statistical significance of the trends in the CMIP5 mean were tested at the 99% (p value of 0.01), 95% (p value of 0.05), and 90% (p value of 0.1) levels. The highest significance value associated with the CMIP5 mean trend is reported.

The total annual mean CMIP5 precipitation over the ECL significantly (p value of 0.01) increases by approximately 16% (80 mm season^{-1}) by the end of the twenty-first century (Fig. 5a). The interquartile range (IQR) and spread between the maximum and minimum values illustrate the model scatter for these annual trends. The minimum lower quartile (Q1) and maximum

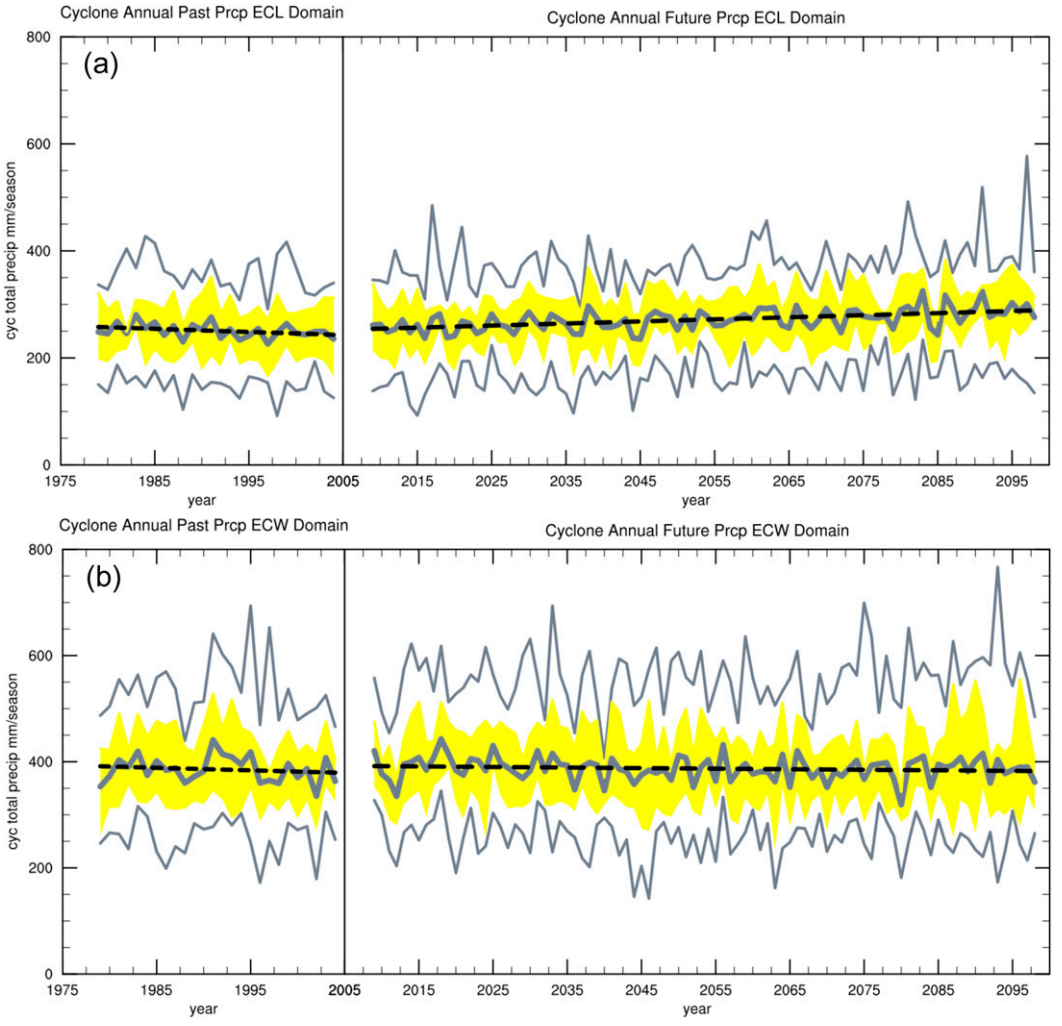

FIG. 6. As in Fig. 5, but for precipitation on cyclone days.

upper quartile (Q3) values over the 125-yr period are ~360 and ~620 mm season^{-1}, respectively, with an IQR ranging between approximately 70 and 200 mm season^{-1} (Fig. 5a). A similar increase (13%) is seen over the adjacent ECW domain (Fig. 5b), though the trend is not statistically significant, in part because of the larger model variability (minimum Q1 of ~600 mm season^{-1}; maximum Q3 of ~980 mm season^{-1}; and IQR of ~50–250 mm season^{-1}). Comparing the ECL and ECW domains, the mean precipitation values over the water domain are about 60% more than over the land domain (Figs. 5a,b).

Figure 6 shows the total annual precipitation for days when a cyclone was present within the domain of interest, which provides insight into the contribution of cyclones to the overall cool season precipitation. On average, approximately 60 cool season days (40%) have been defined as cyclone days. Over the ECL domain, there is a slight decline in cyclone-day precipitation during the historical period, though precipitation significantly (p value of 0.1) increases by 12% (~30 mm season^{-1}) through the twenty-first century (Fig. 6a). For the ECW domain, cyclone-day precipitation declines during the historical period, with essentially no trend (10 mm season^{-1} decrease) through the twenty-first century.

Figure 7 illustrates cool season precipitation for days when no cyclone was detected within the domains. Comparing Figs. 6 and 7, more than half (55%–60%) of the cool season precipitation over ECL and ECW occurs on days when a cyclone is located within the domain. Mean annual noncyclone-day precipitation for the ECL significantly (p level of 0.05) increases by approximately 23% (from ~200 to ~245 mm season^{-1}) by the late twenty-first century (Fig. 7a). For the ECW, noncyclone-day precipitation rises (~80 mm season^{-1}; 24%), though this increase is not statistically significant, with a larger variability among CMIP5 members.

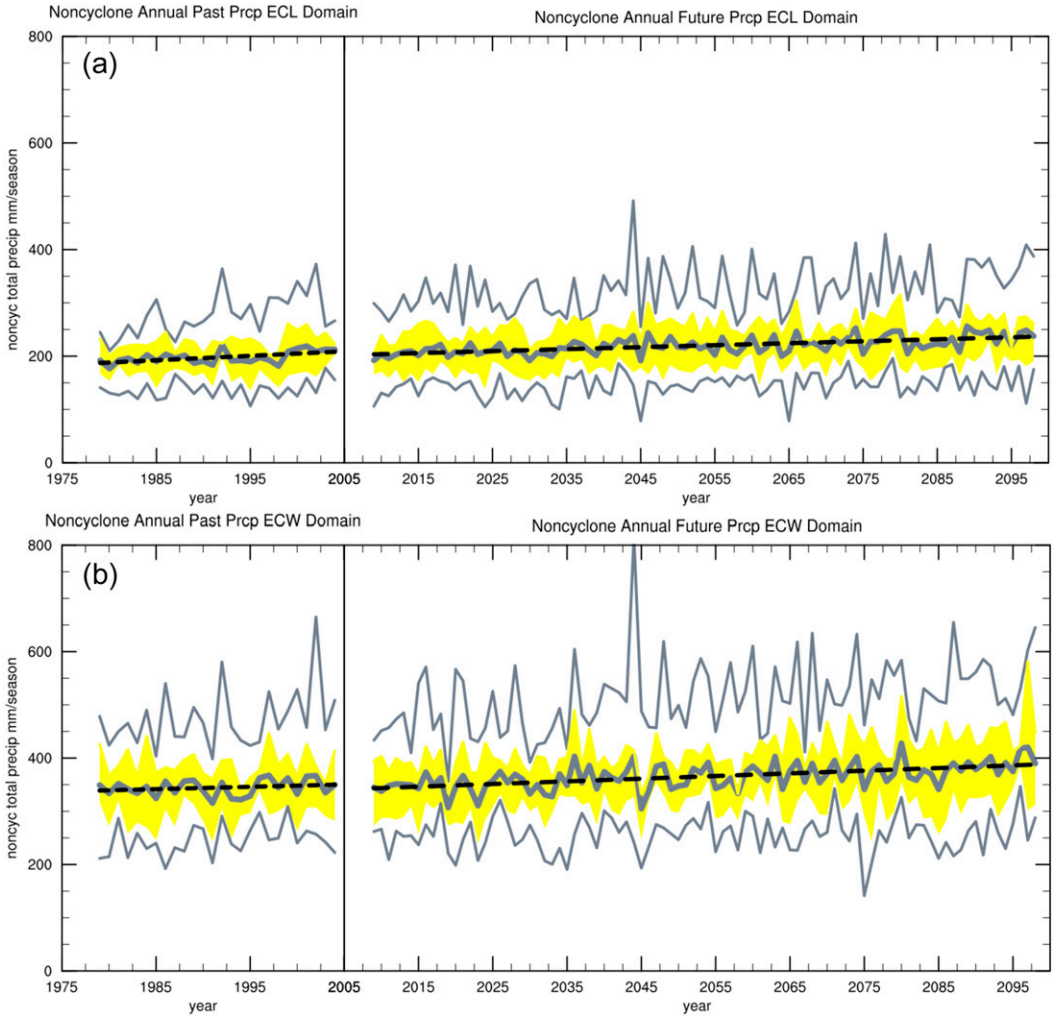

FIG. 7. As in Fig. 5, but for precipitation on noncyclone days.

2) REGIONAL CYCLONE PRECIPITATION

Since cyclones can be responsible for extreme precipitation events over the region, it is important to understand the characteristics of precipitation on cyclone days, as well as the relationship between cyclone-day precipitation and cyclone activity. Figure 8 shows the long-term trends in the daily precipitation over the land and coastal ocean domains on cyclone days, providing the opportunity to isolate the amount of regional precipitation occurring on each cyclone day. While the historical trend is flat over the ECL, there is a 20% (0.8 mm cyclone^{-1}) significant (p value of 0.05) increase in daily cyclone precipitation through the twenty-first century (Fig. 8a). This trend occurs as the number of cyclone days within the ECL domain is projected to decline by about 5 cyclone days per year (p value of 0.05; Fig. 9a) by 2100. Therefore, the cool season precipitation associated with ECL cyclones is projected to increase (Fig. 6a), despite the decrease in the number of cool season cyclones (Fig. 9a).

For the ECW domain, there is essentially no change in the mean daily cyclone precipitation through the historical period (Fig. 8b). In the future century, there is a projected increase of 8% (0.5 mm cyclone^{-1}), though this rise is not statistically significant (Fig. 8b). The number of cyclone days over the eastern U.S. coastal waters is anticipated to decrease by about 8 cyclone days per year by 2100 (Fig. 9b), though this trend lacks statistical significance. Though future projections of daily cyclone precipitation over the ECW domain are not as robust as over the ECL, the rising trend in precipitation associated with coastal cyclones is consistent over both the coastal land and water domains.

With cyclone precipitation projected to increase, it is important to evaluate variations in event intensity and

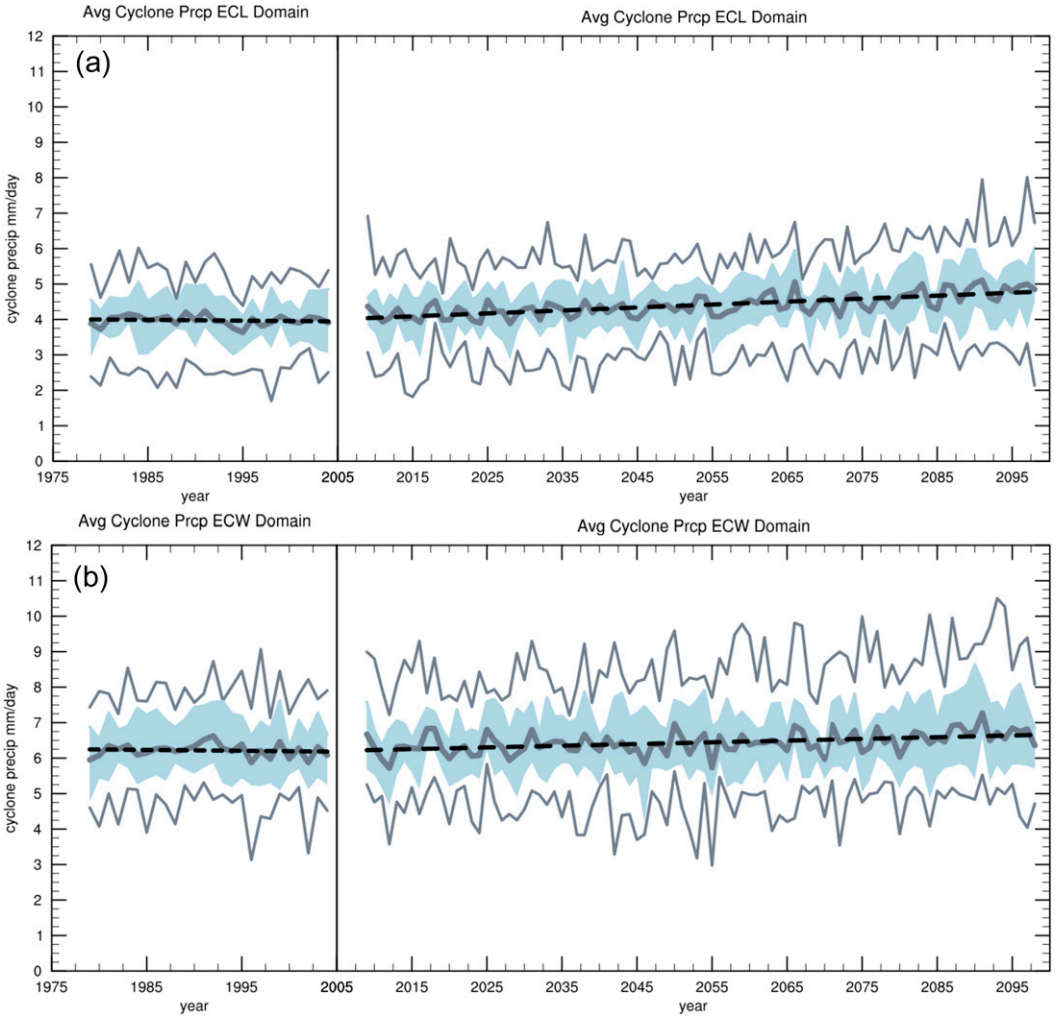

FIG. 8. Daily precipitation (mm cyclone^{-1}) for cool season (November–March) cyclone days over the (a) ECL and (b) ECW domains, for 11 of the 14 CMIP5 models listed in Table 1. The thick gray line is the CMIP5 mean; the top and bottom thin gray lines are the max and min values, respectively; and the blue shading marks the interquartile range. The black dashed line is the trend in the CMIP5 mean. Models include BCC-CSM1.1, CCSM4, CNRM-CM5.1, GFDL-ESM2M, HadGEM2-ES, INM-CM4, IPSL-CM5A-LR, MIROC5, MIROC-ESM, MRI-CGCM3, and NorESM1-M.

identify the events that contribute the most to these trends (i.e., future variations due to a rise in the number of light, moderate, or heavy precipitation events). Figure 10 illustrates the change in the intensity of cyclone-day precipitation events for the early (2009–38; purple), middle (2039–68; yellow), and late (2069–98; red) twenty-first-century time periods compared to the historical period (1979–2004), normalized to represent the change in the number of events per year. For the ECL, there is an approximately 9% decrease (~6 events per year) in the number of the lightest precipitation events (<0.5 mm day^{-1}), with an approximately 22% reduction (~5 fewer events per year) in the 0.5–1.5 mm day^{-1} events by the late twenty-first century (Fig. 10a). The trend for more moderate events (1.5–7.5 mm day^{-1}) is less clear, while there is an increasing trend (30%) in heavier (7.5–9.5 mm day^{-1}) precipitation events (Fig. 10a). For the top 5% of ECL precipitation events (>9.5 mm day^{-1}), there is a 73% increase (~3 events per year) in these extreme events by the end of the century.

Over coastal ocean (ECW), a 5% decrease (3 fewer events per year) in the number of the lightest precipitation events (<0.5 mm day^{-1}) is anticipated, with little change in the 0.5–1.5 mm day^{-1} events (Fig. 10b). For most other precipitation thresholds (1.5–9.5 mm day^{-1}), the number of events is projected to decrease about 10%–17%. Conversely, the frequency of the top 5% of events (>12.5 mm day^{-1}) is anticipated to increase by 21% (~1 event per year) by the late twenty-first century. Therefore, over both the land and water domains, the

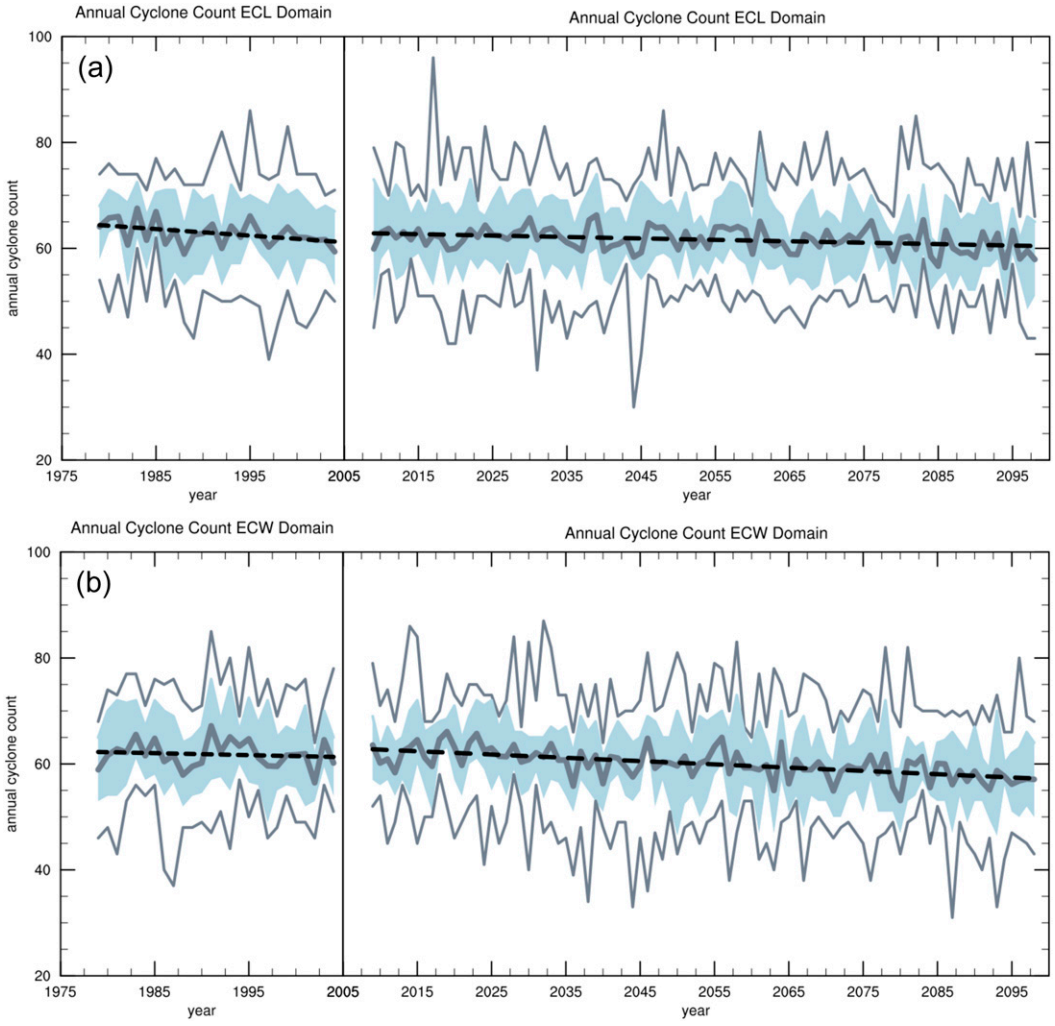

FIG. 9. As in Fig. 8, but for the total number of cool season (November–March) cyclone days.

number of the lightest cyclone-day precipitation events is anticipated to decrease while the most extreme cyclone precipitation events are projected to rise.

4. Discussion and summary

Using historical output from an ensemble of CMIP5 members, this study illustrated the ability of the CMIP5 ensemble to reproduce cool season precipitation over the eastern United States and western North Atlantic Ocean. It also quantified the projected changes in future (RCP8.5) cool season precipitation over two adjacent, topographically varying domains during the total cool season as well as for cyclone days only.

a. Historical precipitation

The distribution of cool season historical CMIP5 mean precipitation over the eastern U.S. and western Atlantic storm track was consistent with observations. For the coastal land regions, precipitation decreased northward, with the largest values near the coastline. Compared to observational products (GPCP, CMAP, and CPC unified), the CMIP5 mean produced more precipitation than the CMAP and less than the GPCP within the northern section of the western North Atlantic storm track. The ensemble mean consistently underrepresented southeastern U.S. precipitation. Over the northeastern United States and parts of the mid-Atlantic, the ensemble mean produced more precipitation than the CMAP and less than the GPCP. Overall, the historical CMIP5 precipitation fell within the range of the three observational datasets, providing confidence in its use for evaluating future trends.

The distribution of historical precipitation intensity was quantified over two adjacent, topographically different domains (ECL and ECW) to highlight differences

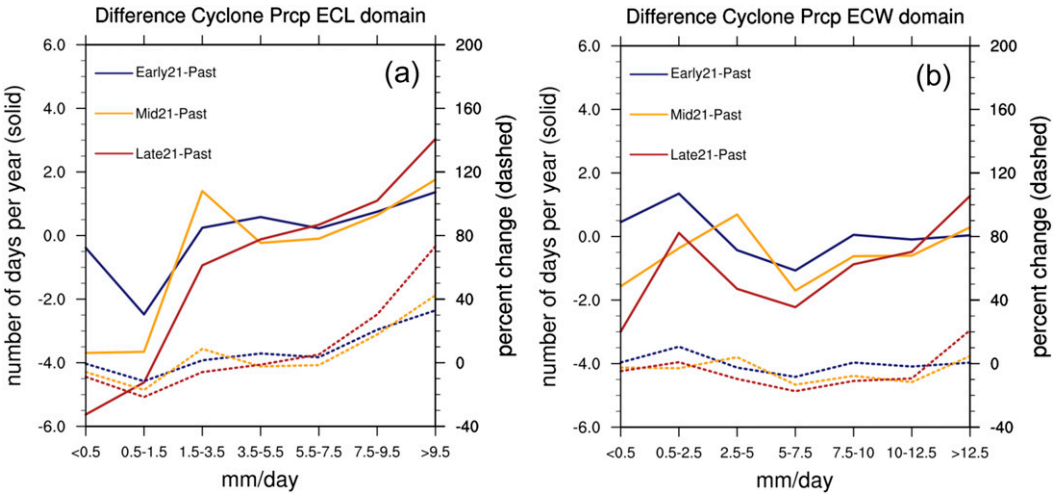

FIG. 10. Difference plot illustrating the change in the number of cyclone-day precipitation events per year between the early twenty-first century and the past (purple solid), the mid-twenty-first century and the past (yellow solid), and the late twenty-first century and the past (red solid), and the percent change for the early twenty-first century and the past (purple dashed), the mid-twenty-first century and the past (yellow dashed), and the late twenty-first century and the past (red dashed) periods for various precipitation thresholds over the (a) ECL and (b) ECW domains.

in precipitation characteristics because of land–ocean gradients. Comparing the historical distribution of precipitation over the ECL and ECW domains, there were half as many of the lightest precipitation events and a quarter more of the most extreme precipitation events over the coastal water domain than the coastal land domain. Cumulatively, there was more accumulated precipitation over the water than the land.

The performance of the individual CMIP5 members was evaluated over the combined ECL and ECW domains, defined as the EC domain, with respect to two observational products, the CMAP and GPCP analyses. The performance of the individual CMIP5 members was not dependent on grid resolution, meaning that the relatively high-resolution members did not perform better than the relatively low-resolution members. This differs from the cyclone analyses performed by Colle et al. (2013). They showed that the relatively high-resolution CMIP5 members more accurately represented the location, track, and intensity of western Atlantic and eastern U.S. cyclones compared to the relatively low-resolution members. This emphasizes the challenges in evaluating the performance of a GCM based on precipitation. While the dynamics in the GCM may be well represented (i.e., accurate intensity and location of a cyclone), the precipitation field may not. Conversely, a GCM may develop an accurate precipitation field, while the dynamics may be poorly represented, indicating that the precipitation field was accurate for some other, potentially misleading, reasons (i.e., compensation by the microphysical scheme in the model). This suggests the ability of a GCM to accurately produce a precipitation field should not be assumed based on its ability to accurately produce dynamical features, such as cyclones.

b. *Future precipitation*

Future projections in cool season regional precipitation were quantified for the ECL and ECW domains. Total cool season CMIP5 mean precipitation over the ECL domain was projected to significantly increase by 16% by the end of the twenty-first century. This is consistent with the projected rise in global atmospheric water vapor (20%; Held and Soden 2006); however, the percent increase in precipitation is half as large as the projected rise in regional saturation vapor pressure over the eastern United States considering regional temperature changes. Under a higher emissions scenario (A1F1), the DJF temperature over the northeastern United States is projected to rise 5.5°C by the 2070–99 period relative to the 1961–90 average (Hayhoe et al. 2007). This yields a 38.5% increase in northeastern U.S. regional vapor pressure based on a 7% K^{-1} increase predicted by the Clausius–Clapeyron equation (Held and Soden 2006). This indicates that the precipitation yield due to an increase in temperature is more complex than predicted by the Clausius–Clapeyron equation (Westra et al. 2013). This is further supported by the estimated 5%–6% increase in global (Wetherald and Manabe 2002) and hemispheric midlatitude (O'Gorman and Schneider 2009) future precipitation by 2100, though the projected increase in atmospheric water vapor is 4 times as large (20%; Held and Soden 2006).

Total cool season precipitation over the ECW was projected to rise by 2100 as well, though the increase was not significant.

Regional changes in precipitation were evaluated on cyclone days and noncyclone days. Over the ECL domain, there was a 12% significant increase in cool season cyclone-day precipitation by 2100, with a 10% larger increase on noncyclone days. The increase in seasonal cyclone-day precipitation occurred despite a decrease in the number of cyclone days. Over the ECW domain, there was no trend in cool season ECW cyclone-day precipitation and the number of cyclone days was projected to decline. For noncyclone days, there was 10% greater increase by 2100 than for cyclone days. Over both domains, the percent increase for noncyclone-day precipitation was greater than for cyclone days, even though cyclones were responsible for a majority of the historical precipitation.

As discussed above, the percent increase in precipitation over the ECL domain was greater than over the ECW domain on cyclone days. Ruosteenoja and Räisänen (2013) showed that, over Europe, the slower future warming of the oceans contributed to a slower increase in the saturation specific humidity and relative humidity than over land. They hypothesized that the increase in environmental moisture contributed to an increase in precipitation. Potentially, a similar mechanism may be contributing to the greater increase in precipitation over land than the coastal ocean in the current study. Future work is required to evaluate the mechanisms that are responsible for this topographically varying precipitation change.

Future variations in regional precipitation per cyclone day over both domains were quantified as well. The amount of precipitation that falls on each ECL cyclone day was projected to significantly rise by 20%, with a smaller 8% increase over the ECW. This rise may be due to a combination of increased atmospheric water vapor content in addition to changes in cyclone intensity and location of the storm track (Pfahl and Wernli 2012). Colle et al. (2013) showed that over the ECL domain, the number of deep cyclones (<980 hPa) was projected to increase by the end of the twenty-first century. Increased available moisture is projected to produce more intense cyclones through additional latent heating and greater precipitation rates (Held 1993; Trenberth 1999). Therefore, while the number of cool season cyclone days may decrease over the northwestern Atlantic storm track, the increase in the number of intense cyclones in conjunction with the increase in atmospheric moisture could result in the increase in precipitation on cyclone days. Complementary to the current study, Bengtsson et al. (2009) showed that the quantity of accumulated precipitation during the most extreme precipitation events is projected to increase as much as 30% within hemispheric storm tracks.

Future variations in the cyclone-day precipitation distribution over the ECL and ECW domains were quantified to evaluate changes in the frequency of light, moderate, and intense precipitation events. The number of the most extreme precipitation events was projected to increase over both domains, while the number of the lightest precipitation events was projected to decrease. This is consistent with Maloney et al. (2014), who showed that the number of relatively heavy precipitation events over the northeastern United States during the entire cool season increased as much as 4–5 times by the late twenty-first century for all cool season days.

Given that cool season precipitation associated with cyclones is projected to increase over the eastern United States and western Atlantic, it would be of interest to understand the dynamics controlling these projected changes. Furthermore, it would be worthwhile to understand the thermodynamic and dynamic processes that contribute to differences in the increase in precipitation over the coastal land and coastal water. This requires additional analyses of future projections in regional atmospheric moisture, cyclone dynamics, and other atmospheric processes (e.g., contribution from orographic lift, cool season convective storms) contributing to precipitation. For example, cyclone-based composites of temporal changes in precipitable water, quasigeostrophic forcing mechanisms, and cyclone structure would be beneficial. Additionally, it would be worthwhile to evaluate the mechanisms contributing to the increase in precipitation on noncyclone days as well.

Acknowledgments. The authors thank anonymous reviewers for improving the quality of this manuscript. The authors acknowledge the support of NOAA/Climate Program Office Modeling, Analysis, Predictions and Projections (MAPP) Program as part of the CMIP5 Task Force under Grant NA11OAR4310104; the DOE Office of Science through its Office of Biological and Environmental Sciences; and the National Sea Grant College Program of NOAA (NYSG R/RCP-17). The authors would also like to acknowledge the World Climate Research Program's Working Group on Coupled Modeling, which is responsible for CMIP, as well as the climate modeling groups listed in Table 1 of this paper for producing and making available their model output. For CMIP, the U.S. Department of Energy's Program for Climate Model Diagnosis and Intercomparison provides coordinating support and led development of software infrastructure in partnership with the Global Organization for Earth System Science Portals.

REFERENCES

Adler, R. F., and Coauthors, 2003: The Version-2 Global Precipitation Climatology Project (GPCP) monthly precipitation analysis (1979–present). *J. Hydrometeor.,* **4,** 1147–1167, doi:10.1175/1525-7541(2003)004<1147:TVGPCP>2.0.CO;2.

Allan, R. P., and B. J. Soden, 2008: Atmospheric warming and the amplification of precipitation extremes. *Science,* **321,** 1481–1484, doi:10.1126/science.1160787.

Allen, M. R., and W. J. Ingram, 2002: Constraint on future changes in climate and the hydrologic cycle. *Nature,* **419,** 224–232, doi:10.1038/nature01092.

Annan, J. D., and J. C. Hargreaves, 2011: Understanding the CMIP3 multimodel ensemble. *J. Climate,* **24,** 4529–4538, doi:10.1175/2011JCLI3873.1.

Arkin, P. A., T. M. Smith, M. R. P. Sapiano, and J. Janowiak, 2010: The observed sensitivity of the global hydrological cycle to changes in surface temperature. *Environ. Res. Lett.,* **5,** 035201, doi:10.1088/1748-9326/5/3/03520.

Arora, V. K., and Coauthors, 2011: Carbon emission limits required to satisfy future representative concentration pathways of greenhouse gases. *Geophys. Res. Lett.,* **38,** L05805, doi:10.1029/2010GL046270.

Bengtsson, L., K. I. Hodges, and E. Roeckner, 2006: Storm tracks and climate change. *J. Climate,* **19,** 3518–3543, doi:10.1175/JCLI3815.1.

——, ——, and N. Keenlyside, 2009: Will extratropical storms intensify in a warmer climate? *J. Climate,* **22,** 2276–2301, doi:10.1175/2008JCLI2678.1.

Brown, P. J., R. S. Bradley, and F. T. Keimig, 2010: Changes in extreme climate indices for the northeastern United States, 1870–2005. *J. Climate,* **23,** 6555–6572, doi:10.1175/2010JCLI3363.1.

Chang, E. K. M., 2013: CMIP5 projection of significant reduction in extratropical cyclone activity over North America. *J. Climate,* **26,** 9903–9922, doi:10.1175/JCLI-D-13-00209.1.

Chen, C.-T., and T. Knutson, 2008: On the verification and comparison of extreme rainfall indices from climate models. *J. Climate,* **21,** 1605–1621, doi:10.1175/2007JCLI1494.1.

Colle, B. A., F. Buonaiuto, M. J. Bowman, R. E. Wilson, R. Flood, R. Hunter, A. Mintz, and D. Hill, 2008: New York City's vulnerability to coastal flooding. *Bull. Amer. Meteor. Soc.,* **89,** 829–841, doi:10.1175/2007BAMS2401.1.

——, Z. Zhang, K. Lombardo, E. Chang, P. Liu, and M. Zhang, 2013: Historical evaluation and future prediction of eastern North American and western Atlantic extratropical cyclones in the CMIP5 models during the cool season. *J. Climate,* **26,** 6882–6903, doi:10.1175/JCLI-D-12-00498.1.

DeAngelis, A. M., A. J. Broccoli, and S. G. Decker, 2013: A comparison of CMIP3 simulations of precipitation over North America with observations: Daily statistics and circulation features accompanying extreme events. *J. Climate,* **26,** 3209–3230, doi:10.1175/JCLI-D-12-00374.1.

Donner, L. J., and Coauthors, 2011: The dynamical core, physical parameterizations, and basic simulation characteristics of the atmospheric component AM3 of the GFDL global coupled model CM3. *J. Climate,* **24,** 3484–3519, doi:10.1175/2011JCLI3955.1.

Dufresne, J,-L., and Coauthors, 2013: Climate change projections using the IPSL-CM5 Earth System Model: From CMIP3 to CMIP5. *Climate Dyn.,* **40,** 2123–2165, doi:10.1007/s00382-012-1636-1.

Field, P. R., and R. Wood, 2007: Precipitation and cloud structure in midlatitude cyclones. *J. Climate,* **20,** 233–254, doi:10.1175/JCLI3998.1.

Gent, P. R., and Coauthors, 2011: The Community Climate System Model version 4. *J. Climate,* **24,** 4973–4991, doi:10.1175/2011JCLI4083.1.

Griffiths, M. L., and R. S. Bradley, 2007: Variations of twentieth-century temperature and precipitation extreme indicators in the northeast United States. *J. Climate,* **20,** 5401–5417, doi:10.1175/2007JCLI1594.1.

Hayhoe, K., and Coauthors, 2007: Past and future changes in climate and hydrological indicators in the US Northeast. *Climate Dyn.,* **28,** 381–407, doi:10.1007/s00382-006-0187-8.

Held, I. M., 1993: Large-scale dynamics and global warming. *Bull. Amer. Meteor. Soc.,* **74,** 228–241, doi:10.1175/1520-0477(1993)074<0228:LSDAGW>2.0.CO;2.

——, and B. J. Soden, 2006: Robust responses of the hydrological cycle to global warming. *J. Climate,* **19,** 5686–1560, doi:10.1175/JCLI3990.1.

Higgins, R. W., J. E. Janowiak, and Y.-P. Yao, 1996: *A Gridded Hourly Precipitation Data Base for the United States (1963-1993).* NCEP/Climate Prediction Center Atlas 1, 46 pp.

——, W. Shi, E. Yarosh, and R. Joyce, 2000: *Improved United States Precipitation Quality Control System and Analysis.* NCEP/Climate Prediction Center Atlas 7, 40 pp.

Hodges, K. I., 1994: A general method for tracking analysis and its application to meteorological data. *Mon. Wea. Rev.,* **122,** 2573–2586, doi:10.1175/1520-0493(1994)122<2573:AGMFTA>2.0.CO;2.

——, 1995: Feature tracking on the unit sphere. *Mon. Wea. Rev.,* **123,** 3458–3465, doi:10.1175/1520-0493(1995)123<3458:FTOTUS>2.0.CO;2.

Horton, R. M., V. Gornitz, D. A. Bader, A. C. Ruane, R. Goldberg, and C. Rosenzweig, 2011: Climate hazard assessment for stakeholder adaptation planning in New York City. *J. Appl. Meteor. Climatol.,* **50,** 2247–2266, doi:10.1175/2011JAMC2521.1.

Insaf, T. Z., S. Lin, and S. C. Sheridan, 2013: Climate trends in indices for temperature and precipitation across New York State, 1948-2008. *Air Qual. Atmos. Health,* **6,** 247–257, doi:10.1007/s11869-011-0168-x.

Jones, C. D., and Coauthors, 2011: The HadGEM2-1000 ES implementation of CMIP5 centennial simulations. *Geosci. Model Dev.,* **4,** 543–570, doi:10.5194/gmd-4-543-2011.

Kharin, V. V., F. W. Zwiers, X. Zhang, and G. C. Hegerl, 2007: Changes in temperature and precipitation extremes in the IPCC ensemble of global coupled model simulations. *J. Climate,* **20,** 1419–1444, doi:10.1175/JCLI4066.1.

Kunkel, K. E., and Coauthors, 2013a: Monitoring and understanding trends in extreme storms: State of knowledge. *Bull. Amer. Meteor. Soc.,* **94,** 499–514, doi:10.1175/BAMS-D-11-00262.1.

——, and Coauthors, 2013b: Regional climate trends and scenarios for the U.S. National Climate Assessment: Part 1. Climate of the Northeast U.S. NOAA Tech. Rep. NESDIS 142-1, 79 pp.

Kutzbach, J. E., J. Williams, and S. Vavrus, 2005: Simulated 21st century changes in regional water balance of the Great Lakes region and links to changes in global temperature and poleward moisture transport. *Geophys. Res. Lett.,* **32,** L17707, doi:10.1029/2005GL023506.

Maloney, E. D., and Coauthors, 2014: North American climate in CMIP5 experiments: Part III: Assessment of twenty-first-century projections. *J. Climate,* **27**, 2230–2270, doi:10.1175/JCLI-D-13-00273.1.

Manabe, S., and R. J. Stouffer, 1980: Sensitivity of a global climate model to an increase of CO_2 concentration in the atmosphere. *J. Geophys. Res.,* **85,** 5529–5554, doi:10.1029/JC085iC10p05529.

——, and R. T. Wetherald, 1980: On the distribution of climate change resulting from an increase in CO_2 content of the atmosphere. *J. Atmos. Sci.,* **37,** 99–118, doi:10.1175/1520-0469(1980)037<0099:OTDOCC>2.0.CO;2.

Mearns, L. O., W. J. Gutowski, R. Jones, L.-Y. Leung, S. McGinnis, A. M. B. Nunes, and Y. Qian, 2009: A regional climate change assessment program for North America. *Eos, Trans. Amer. Geophys. Union,* **90,** 311–312, doi:10.1029/2009EO360002.

Meehl, G. A., C. Covey, T. Delworth, M. Latif, B. McAvaney, J. F. B. Mitchell, R. J. Stouffer, and K. E. Taylor, 2007: The WCRP CMIP3 multimodel dataset: A new era in climate change research. *Bull. Amer. Meteor. Soc.,* **88,** 1383–1394, doi:10.1175/BAMS-88-9-1383.

Novak, D., B. A. Colle, and S. Yuter, 2008: High-resolution observations and model simulations of an intense mesoscale snowband. *Mon. Wea. Rev.,* **136,** 1433–1456, doi:10.1175/2007MWR2233.1.

O'Gorman, P., and T. Schneider, 2009: The physical basis for increases in precipitation extremes in simulations of 21st-century climate change. *Proc. Natl. Acad. Sci. USA,* **106,** 14 773–14 777, doi:10.1073/pnas.0907610106.

Pfahl, S., and H. Wernli, 2012: Quantifying the relevance of cyclones for precipitation extremes. *J. Climate,* **25,** 6770–6780, doi:10.1175/JCLI-D-11-00705.1.

Rotstayn, L. D., M. A. Collier, Y. Feng, H. B. Gordon, S. P. O'Farrell, I. N. Smith, and J. Syktus, 2010: Improved simulation of Australian climate and ENSO-related rainfall variability in a GCM with an interactive aerosol treatment. *Int. J. Climatol.,* **30,** 1067–1088, doi:10.1002/joc.1952.

Ruosteenoja, K., and P. Räisänen, 2013: Seasonal changes in solar radiation and relative humidity in Europe in response to global warming. *J. Climate,* **26,** 2467–2481, doi:10.1175/JCLI-D-12-00007.1.

Scoccimarro, E., S. Gualdi, A. Bellucci, M. Zampieri, and A. Navarra, 2013: Heavy precipitation events in a warmer climate: Results from CMIP5 models. *J. Climate,* **26,** 7902–7911, doi:10.1175/JCLI-D-12-00850.1.

Semenov, V., and L. Bengtsson, 2002: Secular trends in daily precipitation characteristics: Greenhouse gas simulations with a coupled AOGCM. *Climate Dyn,* **19,** 123–140, doi:10.1007/s00382-001-0218-4.

Taylor, K. E., R. J. Stouffer, and G. A. Meehl, 2012: An overview of CMIP5 and the experiment design. *Bull. Amer. Meteor. Soc.,* **93,** 485–498, doi:10.1175/BAMS-D-11-00094.1.

Trenberth, K. E., 1999: Conceptual framework for changes of extremes of the hydrological cycle with climate change. *Climatic Change,* **42,** 327–339, doi:10.1023/A:1005488920935.

——, A. Dai, R. M. Rasmussen, and D. B. Parsons, 2003: The changing character of precipitation. *Bull. Amer. Meteor. Soc.,* **84,** 1205–1217, doi:10.1175/BAMS-84-9-1205.

Voldoire, A., and Coauthors, 2013: The CNRM-CM5.1 global climate model: Description and basic evaluation. *Climate Dyn.,* **40,** 2091–2121, doi:10.1007/s00382-011-1259-y.

Volodin, E. M., N. A. Dianskii, and A. V. Gusev, 2010: Simulating present day climate with the INMCM4.0 coupled model of the atmospheric and coastal general circulations. *Izv. Atmos. Oceanic Phys.,* **46,** 414–431, doi:10.1134/S000143381004002X.

Wake, C., and A. Markham, 2005: Indicators of climate change in the Northeast 2005. Clean Air–Cool Planet Rep., 32 pp.

Watanabe, M., and Coauthors, 2010: Improved climate simulation by MIROC5: Mean states, variability, and climate sensitivity. *J. Climate,* **23,** 6312–6335, doi:10.1175/2010JCLI3679.1.

Wentz, F. J., L. Ricciardulli, K. Hilburn, and C. Mears, 2007: How much more rain will global warming bring? *Science,* **317,** 233–235, doi:10.1126/science.1140746.

Westra, S., L. V. Alexander, and F. W. Zwiers, 2013: Global increasing trends in annual maximum daily precipitation. *J. Climate,* **26,** 3904–3918, doi:10.1175/JCLI-D-12-00502.1.

Wetherald, R. T., and S. Manabe, 2002: Simulation of hydrologic changes associated with global warming. *J. Geophys. Res.,* **107,** 4379, doi:10.1029/2001JD001195.

Xie, P., and P. A. Arkin, 1996: Analysis of global monthly precipitation using gauge observations, satellite estimates, and numerical model predictions. *J. Climate,* **9,** 840–858, doi:10.1175/1520-0442(1996)009<0840:AOGMPU>2.0.CO;2.

——, and ——, 1997: Global precipitation: A 17-year monthly analysis based on gauge observations, satellite estimates, and numerical model outputs. *Bull. Amer. Meteor. Soc.,* **78,** 2539–2558, doi:10.1175/1520-0477(1997)078<2539:GPAYMA>2.0.CO;2.

Xin, X., T. Wu, and J. Zhang, 2012: Introductions to the CMIP 5 simulations conducted by the BCC climate system model (in Chinese). *Adv. Climate Change Res.,* **8,** 378–382.

Yin, X., A. Gruber, and P. Arkin, 2004: Comparison of the GPCP and CMAP merged gauge–satellite monthly precipitation products for the period 1979–2001. *J. Hydrometeor.,* **5,** 1207–1222, doi:10.1175/JHM-392.1.

Yukimoto, S., and Coauthors, 2012: A new global climate model of the Meteorological Research Institute: MRI-CGCM3—Model description and basic performance. *J. Meteor. Soc. Japan,* **90A,** 23–64, doi:10.2151/jmsj.2012-A02.

Zappa, G., L. C. Shaffrey, K. I. Hodges, P. G. Sansom, and D. B. Stephenson, 2013: A multimodel assessment of future projections of North Atlantic and European extratropical cyclones in the CMIP5 climate models. *J. Climate,* **26,** 5846–5862, doi:10.1175/JCLI-D-12-00573.1.

Zhang, Z. S., and Coauthors, 2012: Pre-industrial and mid-Pliocene simulations with NorESM-L. *Geosci. Model Dev.,* **5,** 523–533, doi:10.5194/gmd-5-523-2012.